Available online at www.sciencedirect.com
ScienceDirect
Computers & Fluids 36 (2007) 1106–1118
computers & fluids
www.elsevier.com/locate/compfluid

Numerical simulation of fluid added mass effect on a francis turbine runner

Q.W. Liang [a], C.G. Rodríguez [a], E. Egusquiza [a,*], X. Escaler [a], M. Farhat [b], F. Avellan [b]

[a] Center of Industrial Diagnostics and Fluid Dynamics (CDIF), Technical University of Catalonia, 08028, Av. Diagonal 647, Barcelona, Spain
[b] Laboratory Hydraulic Machinery (LMH), Ecole Polytechnique Federal de Lausanne, CH-1007, Avenue de Cour, 33 bis, Lausanne, Switzerland

Received 20 December 2005; received in revised form 2 June 2006; accepted 13 August 2006
Available online 17 January 2007

Abstract

In this paper, a numerical simulation to analyze the influence of the surrounding water in a turbine runner has been carried out using finite element method (FEM). First, the sensitivity of the FEM model on the element shape and mesh density has been analysed. Secondly, with the optimized FEM model, the modal behaviour with the runner vibrating in air and in water has been calculated. The added mass effect by comparing the natural frequencies and mode shapes in both cases has been determined.

The numerical results obtained have been compared with experimental results available. The comparison shows a good agreement in the natural frequency values and in the mode shapes. The added mass effect due to the fluid structure interaction has been discussed in detail.

Finally, the added mass effect on the submerged runner is quantified using a non-dimensional parameter so that the results can be extrapolated to runners with geometrical similarity.

1. Introduction

With the great improvement of technology and manufacturing level of hydraulic turbine, there is a trend to increase the power concentration of the units. Therefore, the head, fluid velocity and hydraulic force will be increased considerably. Consequently, some severe vibration problems could be induced by design defects or off-design operation, which could lead to serious accidents and badly influence the security in production as well as the stability in the operation of power plants. The vibratory response of the turbines during operation depends largely on the effective dynamic properties of the runners. Therefore, the investigation on dynamic behaviour of turbine runner has been highly regarded and is quite important to approach the solution of vibration problems for turbines in operation. Since the runners are working submerged in water, the dynamic behaviour could be strongly affected by the presence of this heavy fluid. Therefore, the study on turbine runner structures considering water effect has a high practical interest.

An accurate understanding of the dynamic behaviour of an elastic structure submerged in fluid has received extensive attention since the middle of last century. Lindholm et al. [1] experimentally investigated the vibration of cantilever plates in air and in water and the results have been the benchmark for later investigations. Based on chord-wise hydrodynamic strip theory, they also did theoretical predictions by modifying the simple beam theory and thin plate theory to include an empirical correction factor to take into account the added mass for variety of modes. Meyerhoff [2] calculated the added mass of thin rectangular plates in infinite fluid using dipole singularities. Gladwell and Zimmermann [3] and Gladwell and Mason [4] derived

* Corresponding author. Tel.: +34 93 401 25 96; fax: +34 93 401 58 12.
E-mail address: Egusquiza@mf.upc.edu (E. Egusquiza).

0045-7930/$ - see front matter © 2007 Elsevier Ltd. All rights reserved.
doi:10.1016/j.compfluid.2006.08.007

the governing equations of an acoustic and structural system based on energy and complementary energy formulations. The equations were used in conjunction with the finite element method (FEM). The finite element method has also been applied to solve problems for totally or partially submerged elastic plates [5–7]. Recently, Fu and Price [8], based on a linear hydro elasticity theory, also presented their results and discussed the effect of the free surface. Kwak [9] and Liang et al. [10] calculated the non-dimensional added virtual mass for some plates and compared the results with experimental data. Liang et al. [11] adopted an empirical added mass formulation and the Rayleigh-Ritz method to determine the frequencies and mode shapes of submerged cantilever plates. They compared their numerical results with the available experimental results and pertinent literature in air and in water. The effect of the geometrical characteristics was also discussed. Ergin and Ugurlu [12] studied cantilever plates with different geometry and submergence depth to show their effect on the added mass. All the natural frequencies obtained from the above mentioned theoretical investigations have errors varying from 5% to 15%, compared with the experimental measurements. Difference between actual boundary conditions used in experiment and the theoretical ones used in calculation were blamed for this discrepancy.

Although plenty of work has been carried out on this topic, most available investigations, both simulations and experiments, are limited to simple geometrical structures. For a structure with complex geometry, such as a hydraulic turbine runner, most of the limited works we are aware of were done in air; few of them addressed the vibration of the structure submerged in water. Dubas and Schuch [13] used ANSYS, with the model built by isoparametric shell elements, to calculate the natural frequency and mode shape of a Francis runner without considering water effect. The runner was simplified as an assembly of several flat plates and banding rings, thus disagreement existed in their results and some modes were lost. Tanaka [14] presented a frequency reduction ratio of only one mode measured on both prototype and model runner. He believed that the natural frequency will be reduced in water due to the added mass effect and introduced an empirical value 0.2 for the frequency reduction ratio. However, he did not publish more detailed experiment or simulation to discuss the added mass effect. Du and He et al. [15,16] developed a method to consider the water effect on the turbine runner by importing the added mass into the structural dynamic theory. They did a simulation with the mesh including both fluid and structure, and showed some mode shapes and corresponding frequencies. In addition, they calculated the frequency reduction ratio and indicated that the added mass effect depends on the mode shapes of the runner. However, only the fluid between adjacent blades was taken into account, what resulted in some underestimation of the added mass effect. In order to analyze the structural vibration in water using the dynamic characteristics obtained in air, a method was developed by Xiao et al. [17]. In this method, the analogy between the vibration in air and in water was used. The difficulty induced by this method is that the frequency reduction ratio must be gained in advance by experiment. Besides, a Francis turbine runner was numerically studied in air and some modes and frequencies were presented. However, the frequencies in water were estimated by adopting some empirical values instead of being calculated directly. Cao and Chen [18] analyzed, experimentally and theoretically, the vibration of a hydro turbine working in water, but the study was focused only on a single blade instead of the whole runner. Liang and Wang [19] performed some numerical simulation on a Francis turbine runner both in air and in a finite water domain. Results were compared and the frequency reduction rations for different modes were obtained. However, there was no corresponding experimental data to check the accuracy of the simulation results.

According to all the forementioned literatures, the investigations on turbine runner submerged in water were mainly carried out theoretically and with some simplification on the model, while few experimental results were available as a reference to check the theoretical results. Recently, Rodriguez et al. [20] have published a detailed experimental investigation on a reduced scale model of a Francis turbine. Because it was not feasible to measure with the runner inside the machine casing, experiments were carried out with the runner suspended in air and inside a pool of water far away enough to the solid walls.

In an actual turbine, there are some fixed solid boundaries near the runner which can modify the added mass effect. This effect can be enhanced if the gap is small and the deflection against the solid wall is large enough. In a Francis turbine, a very small gap is generally found between the runner band and the casing where the seals are located. Therefore, the boundary effect should be important if the vibration modes produce large band deformation in the radial direction. For other band modes with lower deformation the effect should be less significant.

A numerical analysis to determine the influence of the fluid added mass on the same runner used by Rodriguez et al. [20] is presented in this paper. The simulation was carried out in the same condition of the experiment so that the numerical results could be compared. To perform the simulation, the finite element method (FEM), considering fluid structure interaction (FSI), is used. With one mesh showing good accuracy and convergence, simulations were carried out. The natural frequencies, mode shapes and frequency reduction ratios, obtained by simulation, agree well with experiment and the fluid added mass effect is discussed in detail.

2. Numerical model

2.1. Formulations of fluid structure interaction (FSI)

In theoretical considerations, to take into account the fluid effect on the surrounded vibrating structure, the system has to be treated as a fluid structure interaction prob-

lem. In that case, the structural dynamics equation has to be coupled with the fluid equations.

It is well known that the discretized structural dynamics equation can be formulated as follows:

$$[M_s]\{\ddot{u}\} + [C_s]\{\dot{u}\} + [K_s]\{u\} = \{F_s\} \tag{1}$$

where $[M_s]$ is the structural mass matrix; $[C_s]$, the structural damping matrix; $[K_s]$, the structural stiffness matrix, $\{F_s\}$, the applied load vector, and $\{u\}$, the nodal displacement vector.

In the case of water-structure coupling, the behaviour of the water pressure can be described with the acoustic wave equation, known as Helmholtz's equation

$$\nabla^2 P = \frac{1}{c^2}\frac{\partial^2 P}{\partial t^2} \tag{2}$$

where P is the fluid pressure; c, the sonic speed in the fluid medium; t, time; ∇^2, the Laplacian operator. Eq. (2) is derived from the Navier–Stokes equation of motion and the continuity equation by considering the following assumptions [21]:

- The fluid is slightly compressible (density changes due to pressure variations).
- The fluid is non-viscous (no viscous dissipation).
- The flow is irrotational.
- There is no mean flow of the fluid.
- Changes of mean density and pressure in different areas of the fluid domain remain small.

Since the viscous dissipation has been neglected, the Helmholtz's Eq. (2) is referred to as the lossless wave equation for propagation of pressure in fluids. In case of fluid structure interaction problems, Eqs. (1) and (2) have to be considered simultaneously.

Helmholtz's Eq. (2) can be described in matrix notation by introducing a matrix operator $\{L\}$ as

$$\frac{1}{c^2}\frac{\partial^2 P}{\partial t^2} - \{L\}^{\mathrm{T}}(\{L\}P) = 0 \tag{3}$$

After discretizing Eq. (3) using the Galerkin procedure [22] to obtain the element matrices, it is multiplied by a virtual change in pressure and integrated over the volume of the domain with some manipulation [23] to give

$$\int_{vol}\frac{1}{c^2}\delta P\frac{\partial^2 P}{\partial t^2}\mathrm{d}(vol) + \int_{vol}(\{L\}^{\mathrm{T}}\delta P)(\{L\}P)\mathrm{d}(vol) = \int_S \{n\}^{\mathrm{T}}\delta P(\{L\}P)\mathrm{d}(S) \tag{4}$$

where vol is the volume of domain; $\delta P = \delta P\,(x,y,z,t)$, the virtual change in pressure; S, the surface where the derivative of pressure normal to the surface is applied (a natural boundary condition), and $\{n\}$, the unit normal to the interface S.

The equation for the interaction between the fluid and the structure is derived from the continuity requirement at the interface boundary. The normal displacement of the structure must be identical to that of the fluid. Therefore, the fluid momentum equation yields the following relationships between the normal pressure gradient of the fluid and the normal acceleration of the structure at the fluid structure interface S [23]:

$$\{n\}\cdot\{\nabla P\} = -\rho_0\{n\}\cdot\frac{\partial^2 U}{\partial t^2} \tag{5}$$

where U is the displacement vector of the structure at the interface; ρ_0, the mean fluid density. This equation can also be used at other boundaries. In order to account for the dissipation of energy, if any, present at the fluid boundary, a dissipation term is added to the lossless boundary condition Eq. (5) to get [24,25]

$$\{n\}\cdot\{\nabla P\} = -\rho_0\{n\}\cdot\frac{\partial^2 U}{\partial t^2} - \left(\frac{\beta}{c}\right)\frac{1}{c}\frac{\partial P}{\partial t} \tag{6}$$

where $\beta = \frac{r}{\rho_0 c}$ is the non-dimensional boundary absorption coefficient; r, the characteristic impedance of the material at the boundary.

After substituting matrix notion of Eq. (6) into Eq. (4), the integral is given by

$$\int_{vol}\frac{1}{c^2}\delta P\frac{\partial^2 P}{\partial t^2}\mathrm{d}(vol) + \int_{vol}(\{L\}^{\mathrm{T}}\delta P)(\{L\}P)\mathrm{d}(vol) = -\int_S \rho_0\delta P\{n\}^{\mathrm{T}}\left(\frac{\partial^2}{\partial t^2}U\right)\mathrm{d}(S) - \int_S \delta P\frac{\beta}{c}\frac{\partial P}{\partial t}\mathrm{d}(S) \tag{7}$$

This equation contains the fluid pressure P and the structural displacement U as the dependent variables to solve. The finite element shape functions for the spatial variation of the pressure and displacement components are given by

$$P = \{N_p\}^{\mathrm{T}}\{p\} \tag{8}$$

$$U = \{N_u\}^{\mathrm{T}}\{u\} \tag{9}$$

where $\{N_p\}$ is the element shape function for pressure; $\{N_u\}$, the element shape function for displacements, $\{p\}$, the nodal pressure vector, and $\{u\} = \{u_x\},\{u_y\},\{u_z\}$, the nodal displacement component vectors. Substituting Eqs. (8) and (9) into Eq. (7), the finite element statement of the Helmholtz's Eq. (2) is given by

$$\int_{vol}\frac{1}{c^2}\{\delta p\}^{\mathrm{T}}\{N_p\}\{N_p\}^{\mathrm{T}}\mathrm{d}(vol)\{\ddot{p}\} + \int_{vol}\{\delta p\}^{\mathrm{T}}[B]^{\mathrm{T}}[B]\mathrm{d}(vol)\{p\} + \int_S \rho_0\{\delta p\}^{\mathrm{T}}\{N_p\}\{n\}^{\mathrm{T}}\{N_u\}^{\mathrm{T}}\mathrm{d}(S)\{\ddot{u}\} + \int_S \frac{\beta}{c}\{\delta p\}^{\mathrm{T}}\{N_p\}\{N_p\}^{\mathrm{T}}\mathrm{d}(S)\{\dot{p}\} = 0 \tag{10}$$

where $[B] = \{L\}\{N_p\}^{\mathrm{T}}$, and $\{n\} =$ normal at the fluid boundary.

Invariable terms over the element are taken out of the integration sign. $\{\delta p\}$ is an arbitrarily introduced virtual change in nodal pressure, which can be factored out in

Eq. (10). Since $\{\delta p\}$ is not equal to zero, Eq. (10) can be written in matrix notation to get the discretized Helmholtz's equation [26]

$$[M_f]\{\ddot{p}\} + [C_f]\{\dot{p}\} + [K_f]\{p\} = \{F_{sf}\} \tag{11}$$

where $[M_f] = \frac{1}{c^2}\int_{vol}\{N_p\}\{N_p\}^{\mathrm{T}}\mathrm{d}(vol)$ = the fluid equivalent "mass" matrix, $[C_f] = \frac{\beta}{c}\int_S\{N_p\}\{N_p\}^{\mathrm{T}}\mathrm{d}(S)$ = the fluid equivalent "damping" matrix, $[K_f] = \int_{vol}[B]^{\mathrm{T}}[B]\mathrm{d}(vol)$ = the fluid equivalent stiffness matrix, $\{F_{sf}\} = -\rho_0\int_S\{N_p\}\{n\}^{\mathrm{T}}\{N_u\}^{\mathrm{T}}\mathrm{d}(S)\{\ddot{u}\}$ = the fluid "load" produced by structure displacement at the interface. Here a coupling matrix is introduced that represents the effective surface area associated with each node on the fluid structure interface

$$[R] = \int_S\{N_u\}\{N_p\}^{\mathrm{T}}\{n\}\mathrm{d}(S) \tag{12}$$

Therefore, the fluid load at the interface in Eq. (11) can be described as

$$\{F_{sf}\} = -\rho_0[R]^{\mathrm{T}}\{\ddot{u}\} \tag{13}$$

By considering the fluid pressure acting at the interface, the Eq. (1) for structural dynamics can be written as follows:

$$[M_s]\{\ddot{u}\} + [C_s]\{\dot{u}\} + [K_s]\{u\} = \{F_s\} + \{F_{fs}\} \tag{14}$$

where $\{F_{fs}\}$ = the fluid pressure load vector at the interface, which can be obtained by integrating the pressure over the area of the surface

$$\begin{aligned}\{F_{fs}\} &= \int_S\{N_u\}P\{n\}\mathrm{d}(S)\\ &= \int_S\{N_u\}\{N_p\}^{\mathrm{T}}\{n\}\mathrm{d}(S)\{p\} = [R]\{p\}\end{aligned} \tag{15}$$

By substituting Eqs. (13) and (15) into Eqs. (11) and (14), the complete finite element discretized equations for the fluid structure interaction problem are written in assembled form as [26]

$$\begin{bmatrix}[M_s] & [0]\\ [M_{fs}] & [M_f]\end{bmatrix}\begin{Bmatrix}\{\ddot{u}\}\\ \{\ddot{p}\}\end{Bmatrix} + \begin{bmatrix}[C_s] & [0]\\ [0] & [C_f]\end{bmatrix}\begin{Bmatrix}\{\dot{u}\}\\ \{\dot{p}\}\end{Bmatrix} + \begin{bmatrix}[K_s] & [K_{fs}]\\ [0] & [K_f]\end{bmatrix}\begin{Bmatrix}\{u\}\\ \{p\}\end{Bmatrix} = \begin{Bmatrix}\{F_s\}\\ \{0\}\end{Bmatrix} \tag{16}$$

where $[M_{fs}] = \rho_0[R]^{\mathrm{T}}$ is the equivalent coupling "mass" matrix, and $[K_{fs}] = -[R]$ is the equivalent coupling "stiffness" matrix.

Therefore, for a problem involving fluid structure interaction the fluid element generates all the matrices with subscript f in addition to the coupling matrices $\rho_0[R]^{\mathrm{T}}$ and $[R]$. The matrices with subscript s are generated by the compatible structural element used in the model.

2.2. Reduced model for simulation and nodal diameter (ND)

Structures such as turbine runners show rotational periodicity in the sense that each sector of the structure repeats itself around an axis. If a structure exhibits such a cyclic symmetry, a reduced model including only one sector can be used to calculate the results for the whole structure.

By using this principle, significant economics on computer resource can be made. In addition, the symmetric characteristic of the discrete FEM model can only be guaranteed by using the reduced model. And thus, some important features on dynamic behaviour of such structures can be perfectly expressed [13,27,28].

It is well known that the vibration modes of a cyclic symmetric structure can be classified according to the numbers of its nodal circles (NC) and nodal diameters (ND). Defined by the condition ND = 0, the modes are singlet. These modes are independent of the angular coordinate θ and natural frequencies are distinct. The modes with ND $\neq$ 0 are doublet; they have a pair of mode shapes with the same natural frequency. Each member of such a pair has either sinusoidal or cosinusoidal θ-dependent mode shape. The only difference between them is a spatial phase shift of ϕ

$$\phi = \pi/(2m) \tag{17}$$

where m is the number of ND [29]. The 2ND and 3ND modes of a circular structure are shown here to illustrate the nodal diameters and the relationships between the pairs of doublet modes.

For the modes of the structure studied in this analysis, the nodal circle does not appear. Hence, according to the number of ND, the modes in this paper can be defined as f_{mn}, where the subscript "m" indicates the number of ND and the subscript "n" is a serial number (Fig. 1).

2.3. FEM model and mesh sensitivity analysis

The tested model runner was constructed following the IEC (International Electrotechnical Commission) Standards for international test acceptance and used in a real model test. It is a replica at a reduced scale of 1:10 of a Francis turbine runner with a specific speed of 0.56. The model runner has 17 blades and a diameter of 409 mm. The shape of the runner with the main dimensions is shown in Fig. 2. The material used is a bronze alloy whose properties are given by Table 1. Based on the cyclic symmetrical characteristic of the structure, a sector including one blade and covering an angle of 360/17 degrees was used to do the simulation. The results were expanded to the whole runner.

Before defining the final mesh configuration, the influence of the element shape and of the mesh density was checked. Two types of elements, hexahedral and tetrahedral, were considered. For each element type, four meshes with increasing number of elements were built up. As it can be observed in Table 2, each mesh has approximately the double number of nodes and elements than the preceding one. Moreover, the two sets of meshes with different element type contain a similar number of nodes.

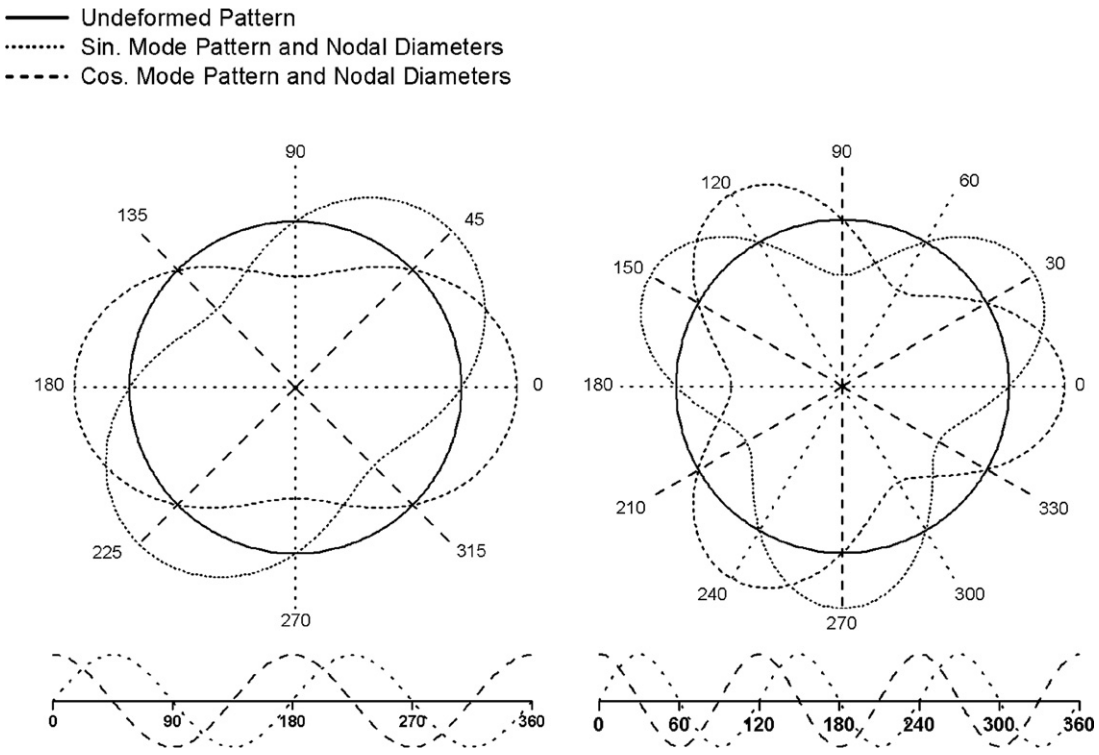

Fig. 1. Modes with 2 and 3 nodal diameters.

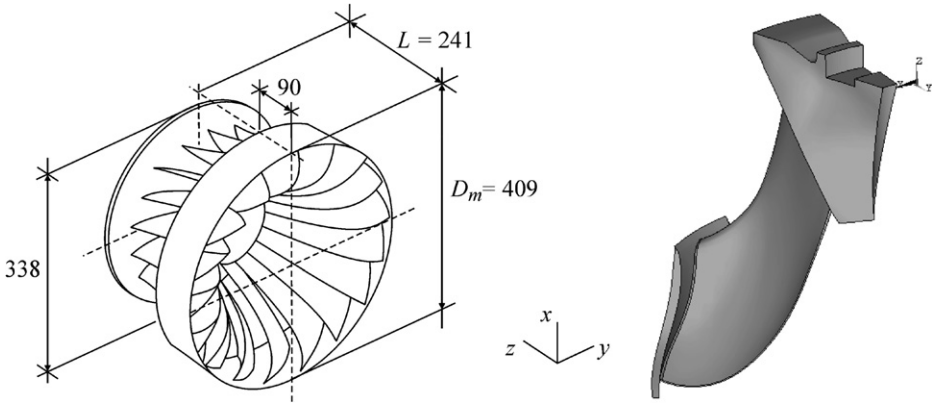

Fig. 2. Geometry of the whole model and one sector.

Table 1
Properties of the runner material

Properties	Young's modulus (GPa)	Density (kg/m^3)	Poisson's ratio
Value	110	8300	0.34

Table 2
Number of elements and nodes in one sector for the four meshes of each element type

	Mesh 1	Mesh 2	Mesh 3	Mesh 4
Element number (Tetra)	4166	6729	13310	25840
Node number (Tetra)	1498	2268	4211	8499
Element number (Hexa)	926	1502	2899	6133
Node number (Hexa)	1472	2298	4179	8529

Comparing the natural frequency results obtained with the different meshes it was observed that, for both tetrahedral and hexahedral element, they converged towards a constant value when the mesh density was increased. In Fig. 3, values of natural frequencies normalized by the final converged value are plotted. It can be noted that the results with hexahedral element converge much faster than the ones with tetrahedral element. In terms of accuracy, the results obtained with the hexahedral element were also found to be closer to the experimental ones. For these reasons, the hexahedral mesh 4 with 6133 elements and 8529 nodes per sector, shown in Fig. 4 expanded to the whole runner, was finally selected to carry out the numerical simulations.

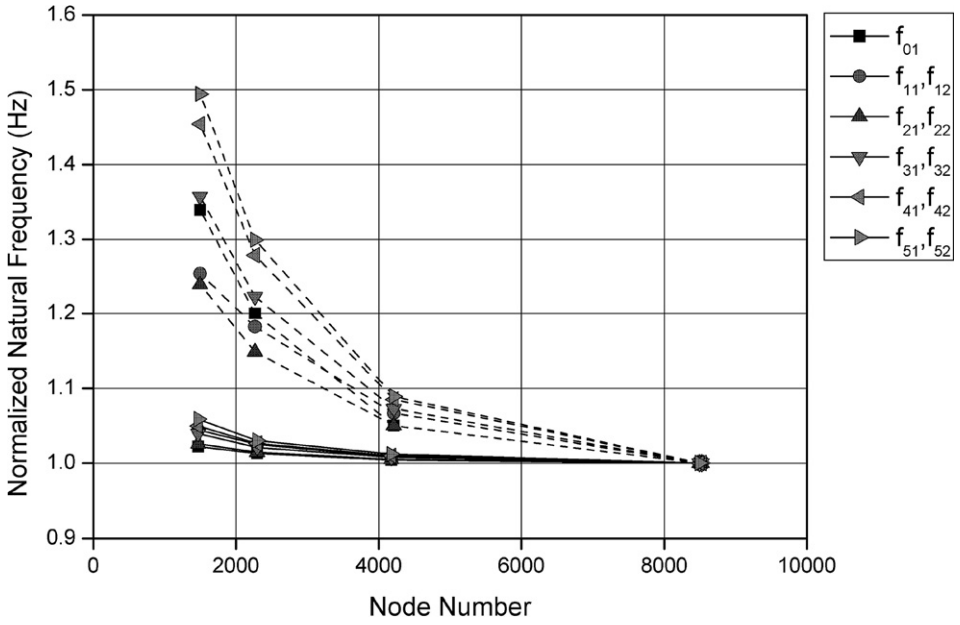

Fig. 3. Results of the mesh sensitivity analysis (Tetra – Dash line; Hexa – Solid line).

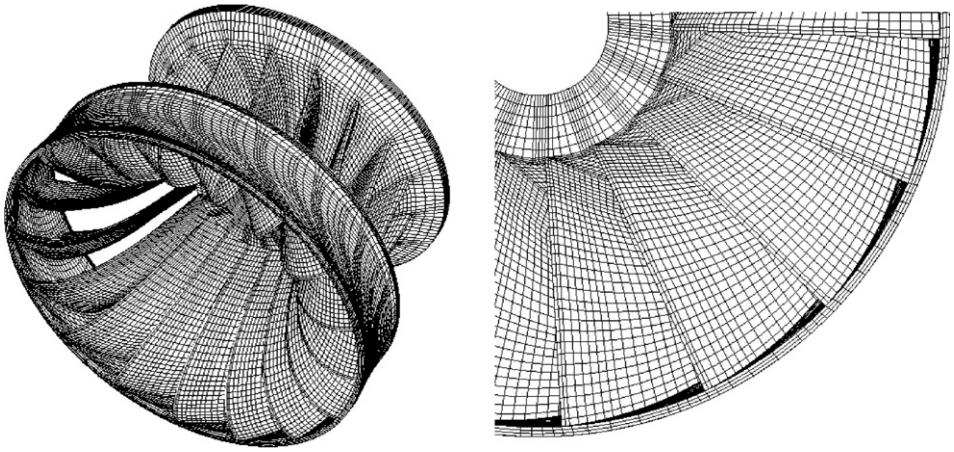

Fig. 4. Discretized finite element mesh with hexahedral element.

3. Evaluation of fluid added mass effect

Fluid added mass effect can be evaluated by comparing the natural frequencies of the runner vibrating in air and in water. Consequently, a detailed modal simulation was carried out to determine the natural frequencies and mode shapes. Since the perfect cyclic symmetry could not be achieved practically, the natural frequencies of the doublet modes obtained by experiment did not repeat at the same value. Nevertheless, these two frequencies are quite similar (maximum difference of 3%, [20]) and the mean values are used for the comparison.

Since the air effect on the experiment was negligible, the corresponding simulation was carried out in vacuum instead of in air. However, in order to avoid the difficulty of expression when comparing, the expression "in air" will be used instead of "in vacuum" in the following discussion.

3.1. Simulation in air

Based on the refined FEM model, the modal characteristics of the free vibration in air were calculated. In Table 3, the natural frequencies obtained with the simulation and experiment are listed. The comparison of the results, including the mode shapes of band, is shown in Fig. 5.

The comparison of simulation with experiment shows a good agreement. Simulation also gives the same mode shapes with the same order. Details about the mode shapes will be discussed later.

Table 3
Natural frequencies of the runner in air (Hz)

	f_{01}	f_{11}, f_{12}	f_{21}, f_{22}	f_{31}, f_{32}	f_{41}, f_{42}	f_{51}, f_{52}
Sim.	425.87	635.53	370.80	485.61	568.18	635.46
Exp.	417.50	616.75	373.50	487.50	573.75	649.75

Note: 1. Sim. = simulation, Exp. = experiment.

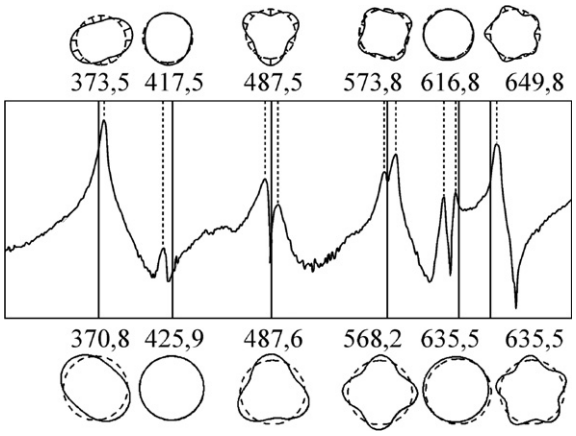

Fig. 5. Comparison between simulation (lower row, Hz) and experiment (upper row, Hz).

3.2. Simulation in water

To make the complete model for the simulation in water, the mesh of the runner was surrounded by a cylindrical fluid domain considering the cyclic symmetric characteristic of the runner. The fluid mesh was extended from the structure mesh so that the same set of nodes was shared between both domains on the interface. The same type of hexahedral element was used to build up the fluid mesh, which contained 29460 nodes and 24137 elements for each sector.

Since the experimental modal analysis of the runner in water was carried out inside a reservoir with free surface [20], the same boundary conditions had to be used in the simulation. These conditions are described by Eq. (6) and must be specified on the boundaries of the FEM model accordingly:

- *Interaction boundary (FSI boundary) on the fluid structure interface:*
  On the fluid structure interface, the displacement of the structure must be identical to that of the fluid in normal direction. Therefore, the equation of motion for fluid particles must be fulfilled at the interface boundary by normal displacements of the structure as described by Eq. (5).
- *Infinite boundary (absorb boundary) on the cylindrical surface:*
  If the dimensions of the fluid are large or infinite, the numerical model has to be cut off at some reasonable distance from the structure. Moreover, the reflection of pressure waves has to be prevented at the cutting boundaries to stop excitation from infinity. One way of doing this is to let the boundary absorb the pressure wave, so that its energy vanishes. This condition can be described by Eq. (6) considering $\beta = 1$.
- *Rigid wall boundary (reflect boundary) on the bottom surface:*
  On the rigid wall, the nodal displacement equals zero. Moreover, the absorption coefficient also equals zero to indicate that there is no energy loss at the boundary. Therefore Eq. (6) can be simplified to the following form to describe this condition:

$$\{n\} \cdot \{\nabla P\} = 0 \tag{18}$$

- *Free surface boundary (opening boundary) on the top surface:*
  The free surface contacts the air where the reference pressure is specified to zero.In Fig. 6, the draft of the model and the FEM mesh are shown. In Table 4, the properties of the water in normal temperature and pressure used are listed.Like in air, the results in water have rather accurate natural frequencies compared with experimental ones, as described in Table 5. The mode shapes are similar to those derived from simulation in air, so here they are avoided to be repeated.

3.3. Accuracy checking

In order to check the accuracy of the simulation with the experimental results, deviation between the simulation and experiment were calculated with Eq. (19), listed in Table 6.

$$\Delta(\%) = [(U_{\text{Sim.}} - U_{\text{exp.}})/U_{\text{exp.}}] \times 100 \tag{19}$$

where $\Delta(\%)$ is the deviation in percent, $U_{\text{Sim.}}$ and $U_{\text{exp.}}$ indicate the results obtained by simulation and by experiment sequentially.

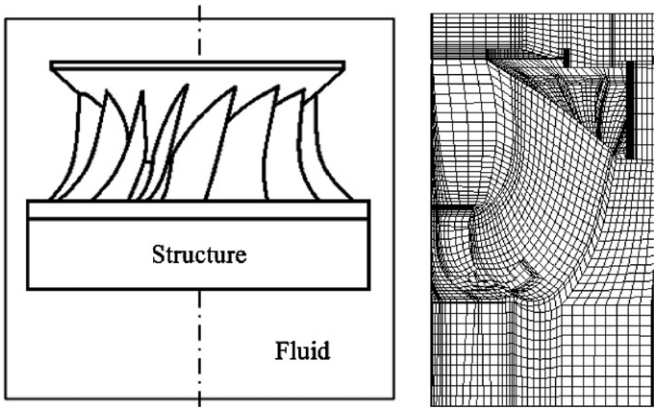

Fig. 6. Fluid domain around the runner and the FEM mesh.

Table 4
Properties of the fluid

Properties	Sonic speed (m/s)	Density (kg/m^3)
Value	1483	1000

Table 5
Natural frequencies of the runner submerged in water (Hz)

	f_{01}	f_{11}, f_{12}	f_{21}, f_{22}	f_{31}, f_{32}	f_{41}, f_{42}	f_{51}, f_{52}
Sim.	383.28	498.90	280.17	335.49	362.34	387.89
Exp.	370.50	481.50	279.50	331.25	359.00	400.00

Table 6
Deviations of simulation compared with experiment (%)

	f_{01}	f_{11}, f_{12}	f_{21}, f_{22}	f_{31}, f_{32}	f_{41}, f_{42}	f_{51}, f_{52}
Natural frequency (in air)	2.00	3.04	−0.72	−0.39	−0.97	−2.20
Natural frequency (in water)	3.45	3.61	0.24	1.28	0.93	−3.03

It can be clearly noticed that almost all deviations remain in a range of ±3.5%. Moreover the mode shapes in air and in water are similar, which also represent good consistency between simulation and experiment (Fig. 5). Accordingly, the simulation can be accepted to be accurate enough to detect well the fluid added mass effect on such a turbine runner by calculating the modal characteristics.

4. Discussion on the results

4.1. Fluid added mass effect by frequency comparison

Due to the effect of the added mass induced by the surrounding water, a significant decrease of the natural frequencies can be observed by comparing the results in air and in water. In Fig. 7, the comparison of the simulation with the experimental results is shown.

The fluid added mass effect can be estimated by calculating the frequency reduction ratio δ of each mode, defined as Eq. (20):

$$\delta = (f_a - f_w)/f_a \tag{20}$$

where f_w and f_a are the natural frequencies in water and in air respectively. The reduction ratios here, calculated by frequency values given in previous paragraphs, are also quite close to the experimental ones, which can be seen in Table 7. And the reduction ratio has been plotted in Fig. 8.

Table 7
Frequency reduction ratio of the runner

	f_{01}	f_{11}, f_{12}	f_{21}, f_{22}	f_{31}, f_{32}	f_{41}, f_{42}	f_{51}, f_{52}
Sim.	0.10	0.21	0.24	0.31	0.36	0.39
Exp.	0.11	0.22	0.25	0.32	0.37	0.38

It can be clearly noticed that the natural frequencies are considerably reduced by the presence of fluid. The frequency reduction ratio does not remain constant for all modes, but varies significantly in a range of 0.10–0.39 depending on the corresponding mode shape.

From Table 7 and Fig. 8, it can also be seen that the reduction ratio for the mode f_{01} is the minimum one (0.10) and goes up with increasing ND. Due to the different effect of the added mass in each mode, the order of some modes does shift in water. The 0 ND mode has a lower frequency than the 3 NDs mode in water while in air its frequency is higher than the 4 NDs mode. However, the order of the modes with one or more NDs remains unchanged in air and in water.

4.2. Determination of fluid added mass effect

The fluid added mass effect can be physically explained based on energy theory. According to the conservation of energy, the total energy of the vibration system remains constant in different mediums, therefore

$$(E_{\text{total}})_{\text{air}} = (E_{\text{total}})_{\text{water}} \tag{21}$$

Here E_{total} indicates the total energy of the vibrating system, involving the potential energy and the kinetic energy. The maximum potential energy equals the maximum kinetic energy.

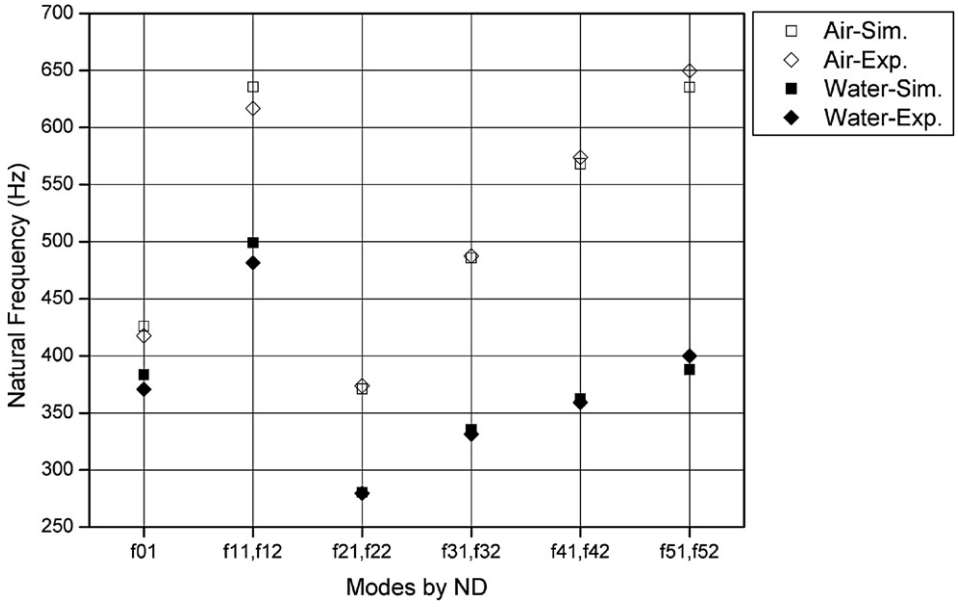

Fig. 7. Natural frequencies in air and in water.

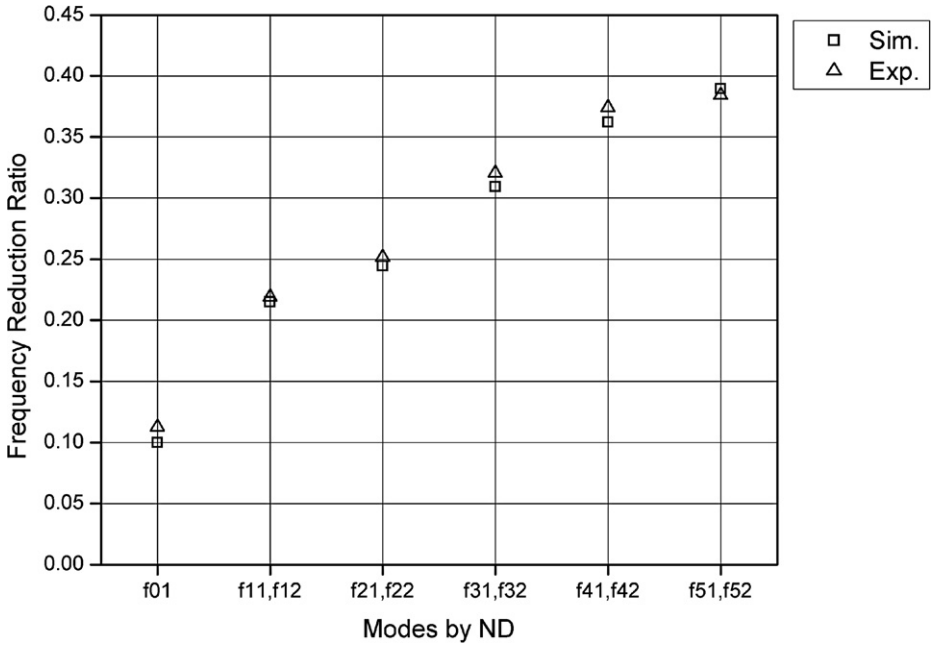

Fig. 8. Comparison of frequency reduction ratios obtained by simulation and experiment.

Moreover, when comparing the response in air with the one in water, only small changes in the mode shapes can be observed. This has been carefully investigated and well verified by some previous publications [11,30–32]. This has been also confirmed by the results found in this investigation when comparing the normalized maximum displacement of the different parts of the runner (Table 11).

Since the mode shapes in air and in water are verified to be the same, the maximum potential energy is not changed when evaluated in air and in water. Consequently, the maximum kinetic energy of the vibrating system remains invariant. When vibrating in water, the structure will lose some kinetic energy to increase the kinetic energy of the attached water, by applying work against the force of the water. Thus, the velocity of structural vibration will decrease and so does the frequency.

With this assumption, the frequencies in water can be related to the frequencies in air, using the following equations [11,32]. The squares of circular frequencies of structure in air (ω_a) and in water (ω_w) can be expressed as

$$\omega_a^2 = (P_s/K_s^*)_{\text{air}} \tag{22}$$

$$\omega_w^2 = (P_S/(K_S^* + K_F^*))_{\text{water}} \tag{23}$$

here the subscript "a" indicates parameters in air while "w" indicates those in water; subscript "S" indicates structure while "F" indicates fluid. P_S is the maximum potential energy of the structure and K_S^* is its reference kinetic energy, which also remains unchanged in air and in water. K_F^* is the equivalent reference kinetic of added water. Hereby

$$\frac{f_w}{f_a} = \frac{\omega_w}{\omega_a} = \frac{1}{\sqrt{1+\lambda}} \tag{24}$$

$$\lambda = \frac{K_F^*}{K_S^*} \tag{25}$$

Reference kinetic energy can be described with modal mass and mode shapes

$$K^* = M \int_V W^2(x,y,z)\mathrm{d}V \tag{26}$$

where M is the modal mass, and $W(x,y,z)$ is a function of the displacements in a three-dimensional rectangular coordinate system, which indicate the mode shape, V is the volume of the structure. To evaluate the effect of the present fluid, an equivalent virtual added mass can be introduced. Then, the added mass can be theoretically assumed to be evenly attached to the plasmids of the structure. Substituting Eq. (26) into Eq. (25) and taking into account the similarity of mode shapes in air and in water, the following equations can be derived:

$$\lambda = \frac{M_a}{M} \tag{27}$$

where M is the modal mass and M_a is the equivalent added mass. It is believed that the added mass factor λ only depends on the material density of the structure ρ_S, on the density of fluid ρ_F, and on the mode shapes [11,33]. By using a subscript "i" to indicate the different mode, the non-dimensional added mass factor for each mode can be expressed as:

$$\gamma_i = \frac{M_{a,i}}{M_i}\frac{\rho_S}{\rho_F} \tag{28}$$

here γ_i is the non-dimensional added mass factor, which remains constant for a specified mode (i), classified by the features of the mode shape (ND, etc.). The non-dimensional added mass depends only on the geometrical characteristics of the structure, which is determined by the design of the runner. In other words, the relationships between

Table 8
Results of modal analysis on a Francis turbine runner

Mode	f_a	f_w	δ	λ	γ_i
f_{01}	425.87	383.28	0.10	0.23	1.95
f_{11}, f_{12}	635.53	498.90	0.21	0.62	5.17
f_{21}, f_{22}	370.80	280.17	0.24	0.75	6.24
f_{31}, f_{32}	485.61	335.49	0.31	1.10	9.09
f_{41}, f_{42}	568.18	362.34	0.36	1.46	12.11
f_{51}, f_{52}	635.46	387.89	0.39	1.68	13.98

natural frequencies in air and in water, obtained by the method employed in this simulation, can also be valid for any other Francis turbine runners with geometrical similarity. This can be practically used to estimate the natural frequencies of other geometrically similar turbine runners constructed with different materials and dimensions.

All the results of this simulation, including natural frequencies in air (f_a) and in water (f_w), frequency reduction ratios (δ), added mass ratios (λ) and the non-dimensional added mass factors (γ_i), are listed in Table 8.

4.3. Features of mode shapes

The fluid added mass effects on the structure are determined by the mode shapes of structure vibrating in water. Therefore, to understand the fluid added mass effects, the essential point is to capture the features of the mode shapes.

Features of mode shapes are determined by the features of the structure. Owing to the geometrical characteristics of Francis turbine runners, the vibration modes of these complex structures imply complex movements. All parts are deformed simultaneously and influence each other.

Since the crown generally has small displacements, the mode shapes can be described by the behaviour of the band and the blades. To order the mode shapes of the whole runner, the number of nodal diameter (ND) in the band is used as the criterion. Here in this investigation, only the modes with number of ND varying from 0 to 5 are studied.

Table 9
Behaviour of the band

Number of ND	Band behaviour	Deformation
0	Torsion, around the axis of rotation	No
0	Elevation, in axial direction	No
1	Swing, in both radial and axial directions, like a pendulum	Yes
2, 3, 4, 5, etc.	Bending, with deformation in radial direction	Yes

For the modes with 0ND, the band behaves without deformation because all the nodes of the band have the same displacement in the same direction. The displacement is in either the radial or the axial direction, performing torsion or elevation motion respectively. For the modes with 1ND, the band swings and there is displacement in both radial and axial directions. For the modes with 2 or more NDs, the band has bending with deformation in the radial direction. In Table 9, the specific characteristics of the band behaviour for each mode with a certain number of ND are summarized.

For Francis turbine runners, the torsion and bending mode generally correspond to lower frequencies, while swing and elevation mode occurs at higher frequencies.

Similarly, the behaviour of blades can be distinguished with nodal lines (NL), or at least with lines of small displacement. Nodal lines on blades can appear parallel to the chord of the blade (from leading edge to trailing edge), or, parallel to the span (from crown to band). Both nodal lines may appear together in some high frequency modes.

Here in the available results of this investigation, the extracted modes are limited to the frequency range of the experiment. The corresponding mode shapes in air and in water present the same features, as are described in Table 10.

Table 10
Features of mode shapes in air

f_a (Hz)	f_w (Hz)	ND	Descriptions of mode shape
425.87	383.28	0	Singlet torsion mode All blades have the same deformation. 1 NL appears around the middle of the blade parallel to the chord
635.53	498.90	1	Doublet swing mode with repeated frequencies, $\phi = \pi/2$ Blades can approximately be separated into two groups. Deformation appears in phase on blades inside each group but counter phase between the two groups. 1 NL appears on the blade parallel to the chord and shifts from crown to band on the blades inside each group
370.80	280.17	2	Doublet bending mode with repeated frequencies, $\phi = \pi/4$ Blade behaviour is similar to 1 ND mode. The blades are separated into 4 groups. Deformation appears in phase on blades inside each group but counter phase between every two adjacent groups. The blades spaced by the angle of $(2\pi/\mathrm{ND})$ present approximate repeatability
485.61	335.49	3	Doublet bending mode with repeated frequencies, $\phi = \pi/6$ Blades behaviour is similar to 2 NDs mode, but separated into 6 groups
568.18	362.34	4	Doublet bending mode with repeated frequencies, $\phi = \pi/8$ Blades behaviour is similar to 2 NDs mode, but separated into 8 groups
635.46	387.89	5	Doublet bending with repeated frequencies, $\phi = \pi/10$ Blades behaviour is similar to 2 NDs mode, but separated into 10 groups

Table 11
Displacement normalized by the maximum displacement in each mode

	f_{01}	f_{11}, f_{12}	f_{21}, f_{22}	f_{31}, f_{32}	f_{41}, f_{42}	f_{51}, f_{52}
Band in air	0.95	0.23	0.85	0.57	0.42	0.33
Blade in air	1.00	1.00	1.00	1.00	1.00	1.00
Crown in air	0.86	0.16	0.11	0.03	0.01	0.00
Band in water	0.91	0.21	0.80	0.53	0.39	0.30
Blade in water	1.00	1.00	1.00	1.00	1.00	1.00
Crown in water	0.82	0.15	0.09	0.04	0.01	0.00

In Table 11, the maximum displacement of each part, normalized by the maximum value of the whole runner, is shown. In all modes obtained by this analysis, the maximum displacement appears on the blades. The thin trailing edges of blades have much larger displacement than the leading edges. In addition, there is also a high displacement in the band, although it is a little lower than in the blades. Displacement on the crown is negligible compared with that on blades and band. In addition, by comparing the normalized maximum displacement on each part in air and in water, it can also be observed that the mode shapes remain almost unchanged.

In order to visualize the mode shapes more clearly, the displacement of the band and blades seen from the bottom is presented in Figs. 9 and 10. The main features about some mode shapes of band and blades, discussed in Table 10, can be observed here.

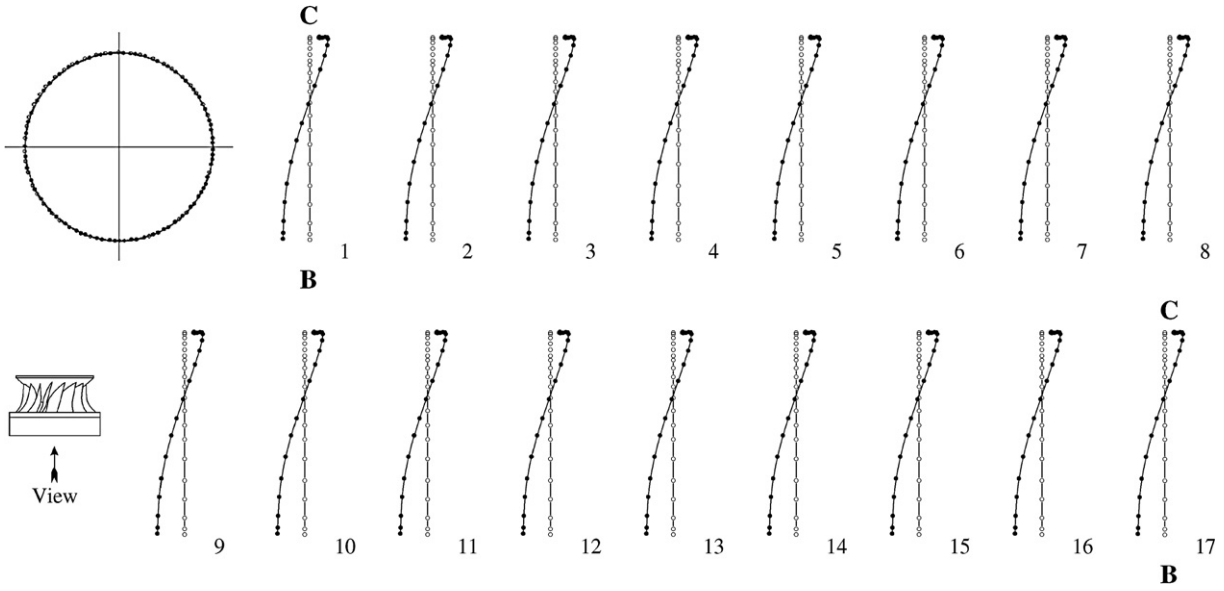

Fig. 9. Displacement of band and blades seen from the bottom for f_{01} (torsion); C– crown, B – band.

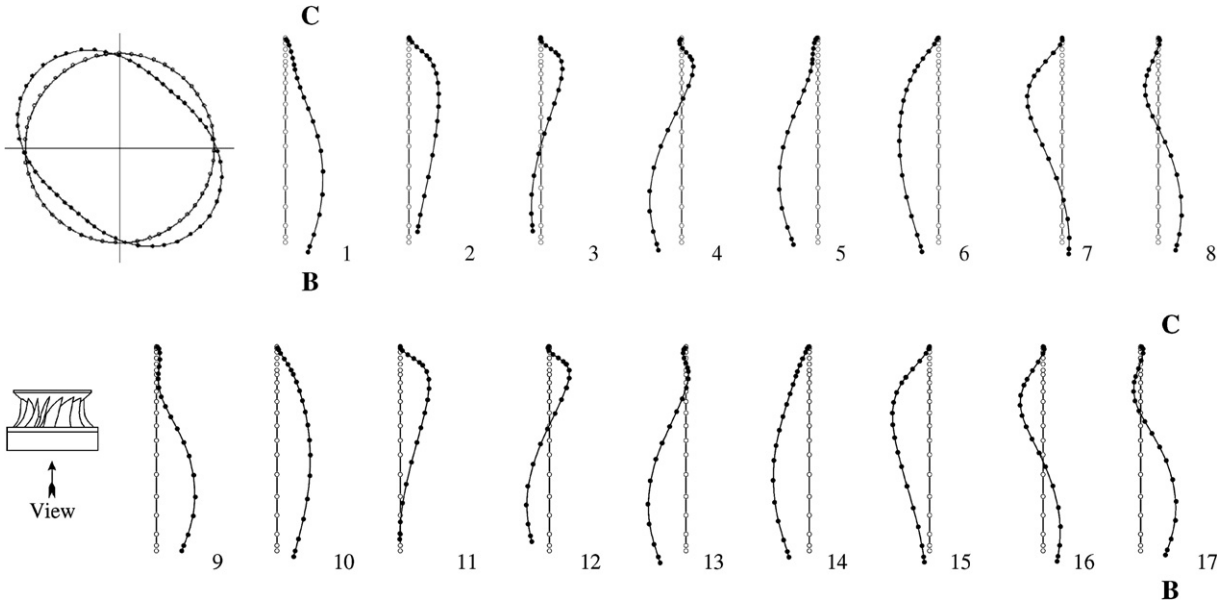

Fig. 10. Displacement of band and blades seen from the bottom for f_{21} (bending); C – crown, B – band.

In this mode (f_{01}), the behaviour of band is a circumferential torsion. It can be seen that all blades have the same deformation with one NL in each blade near the middle position. In addition, it can be observed that the displacement in the crown is lower than in the band and in the opposite direction.

In this mode (f_{21}), the band deforms like an ellipse. The blades can be classified into four groups according to the deformation pattern. The deformation of each blade is approximately repeated every 180° (about 8 blades); such as blade (1) and blade (9), blade (2) and blade (10), etc. One NL appears on most blades. The crown remains undeformed.

5. Conclusions

The added mass effects of the water on a Francis turbine runner using numerical modal analysis were determined with FEM method considering the structure and the surrounding fluid domain. To get a high quality model, sensitivity analyses on the element shape and mesh density were carried out. From these analyses an optimized model with 6133 elements and 8529 nodes for every structural cyclic sector was obtained. And hexahedral elements were used overcoming the difficulties due to the complex geometry of the structure.

To check the accuracy of the simulation, natural frequencies and mode shapes were calculated and compared with the corresponding experimental results. Simulation shows an excellent agreement with experiment. Mode shapes are similar to experimental ones and the maximum deviation in the natural frequencies is around $\pm 3.5\%$.

The added mass effect of the surrounding water has been evaluated by comparing the frequencies in air and in water. Natural frequencies are considerably reduced by the presence of water. The reduction ratio varies in a range of $0.10 \sim 0.39$, depending on the mode shapes.

The added mass effect is physically explained based on the energy theory. A non-dimensional added mass factor is derived, which can be practically extrapolated to estimate the natural frequencies of geometrically similar runners with different materials and dimensions.

To describe the mode shapes precisely, some classifications have been developed based on the number of nodal diameters in the band and on the nodal lines in the blades. The features of mode shapes on each part of the runner were studied and compared carefully. It can be shown that between air and water, although frequencies decrease significantly, the mode shapes undergo only small changes. Blade and band present high displacement amplitude, while in the crown it is negligible. The maximum displacement amplitude appears on the trailing edge of blades in all obtained modes.

Moreover, the method used in this investigation has been proved to be to be valid, which can be used to numerically study the dynamic behaviour of any other hydraulic turbine runner.

Acknowledgements

This research has been carried out as a part of the Hydrodyna Eureka project no. 3246. The authors would like to acknowledge the LMH (EPFL) of Lausanne (Switzerland) and VOITH-SIEMENS Hydro Power Generation of Heidenheim (Germany) for their collaboration. Acknowledgement is also given to Alfa II project "VICONDIA".

References

[1] Lindholm US et al. Elastic vibration characteristics of cantilever plates in water. J Ship Res 1965;9(1):11–22.
[2] Meyerhoff WK. Added masses of thin rectangular plates calculated from potential theory. J Ship Res 1970;14(2):100–11.
[3] Gladwell GML, Zimmermann G. On energy and complementary energy formulations of acoustic and structural vibration problems. J Sound Vibrat 1966;3:233–41.
[4] Gladwell GML, Mason V. Variational finite element calculation of the acoustic response of a rectangular panel. J Sound Vibrat 1971; 14(1):115–35.
[5] Muthuveerappan G, Ganesan N, Veluswami MA. Note on vibration of a cantilever plate immersed in water. J Sound Vibrat 1979;63(3): 385–91.
[6] Rao PS, Sinha G, Mukhopadhyay M. Vibration of submerged stiffened plates by the finite element method. Int Shipbuilding Progr 1993;40(423):261–92.
[7] Volcy GC, et al. Some studies and researches related to the hydroelasticity of steel work. In: Proc. 122nd EUROMECH Colloquium on Numerical Analysis of the Dynamics of Ship Structures 1979; p. 403–36.
[8] Fu Y, Price WG. Interactions between a partially or totally immersed vibrating cantilever plate and the surrounding fluid. J Sound Vibrat 1987;118(3):495–513.
[9] Kwak MK. Axisymmetric vibration of circular plates in contact with fluid. J Sound Vibrat 1991;146(3):381–9.
[10] Liang CC, Tai YS, Li PL. Natural frequencies of annular plates having contact with fluid. J Sound Vibrat 1999;228(5):1167–81.
[11] Liang CC et al. The free vibration analysis of submerged cantilever plates. Ocean Eng 2001;28(9):1225–45.
[12] Ergin A, Ugurlu B. Linear vibration analysis of cantilever plates partially submerged in fluid. J Fluids Struct 2003;17(7):927–39.
[13] Dubas M, Schuch M. Static and dynamic calculation of a francis turbine runner with some remarks on accuracy. Comput Struct 1987; 27(5):645–55.
[14] Tanaka H. Vibration behaviour and dynamic stress of runners of very high head reversible pump-turbines. in the 15th IAHR Symposium. 1990, Belgrade.
[15] Du JB, He SJ, Wang XC. Dynamic analysis of hydraulic turbine runner and balde system (ii) – analysis of examples. J Tsinghua Univ (Sci& Tech) 1998;38(8):72–5.
[16] He SJ, Du JB, Wang XC. Dynamic analysis of hydraulic turbine runner and balde system (i) – mechanics model and formulation. J Tsinghua Univ (Sci& Tech) 1998;38(8):68–71.
[17] Xiao RF et al. Study on dynamic analysis of the francis turbine runner. J Large Elect Machine Hydraulic Turb 2001;7:41–3.
[18] Cao JM, Chen CL. Analysis of abnormal vibration of a large francis turbine runner and cracking of the blades. J South West Jiao Tong Univ 2002;37:68–72.
[19] Liang QW, Wang ZW. Strength and vibration analysis of a francis turbine. J Tsinghua Univ (Sci&Tech) 2003;43(12):1649–52.
[20] Rodriguez CG, Egusquiza E, Escaler X, Liang QW, Avellan F. Experimental investigation of added mass effects on a Francis turbine runner. J Fluids Struct 2006;22(5):699–712.

[21] Kinsler LE et al. Fundamentals of acoustics. New York: John Wiley and Sons; 1982.
[22] Bathe KJ. Finite element procedures. Englewood Cliffs: Prentice-Hall; 1996.
[23] Zienkiewicz OC, Newton RE. Coupled vibrations of a structure submerged in a compressible fluid. In: Symposium on Finite Element Techniques. 1969. University of Stuttgart, Germany.
[24] Craggs A. Finite element model for acoustically lined small rooms. J Sound Vibrat 1986;108(2):327–37.
[25] Rajakumar C, Ali A. Acoustic boundary element eigenproblem with sound absorption and its solution using lanczos algorithm. Int J Numer Meth Eng 1993;36(23):3957–72.
[26] Woyjak DB. Acoustic and fluid structure interaction, a revision 5.0 tutorial. Houston: Swanson Analysis Systems, Inc.; 1992.
[27] Thomas DL. Dynamics of rotationally periodic structures. Int J Numer Meth Eng 1979;14(1):81–102.
[28] Zienkiewicz OC, Scott FC. On the principle of repeatability and its application in analysis of turbine and pump impellers. Int J Numer Meth Eng 1972;4(3):445–50.
[29] Kim M, Moon J, Wickert JA. Spatial modulation of repeated vibration modes in rotationally periodic structures. J Vibrat Acoust Trans ASME 2000;122(1):62–8.
[30] Meirovitch L. Elements of vibration analysis. New York: McGraw-Hill; 1986.
[31] Amabili M. Modal properties of annular plates vibrating in water. In: First International Conference on Vibration Measurements by Laser techniques: Advances and Applications. 1994. Ancona, Italy.
[32] Amabili M, Frosali G, Kwak MK. Free vibrations of annular plates coupled with fluids. J Sound Vibrat 1996;191(5):825–46.
[33] Blevins RD. Formulas for natural frequencies and mode shape. Melbourne: Krieger Publishing Company; 1995.